INTERNATIONAL JOURNAL OF OPTIMIZATION IN CIVIL ENGINEERING
Int. J. Optim. Civil Eng., 2020; 10(1):117-135

TOPOLOGY OPTIMIZATION OF STIFFENED STEEL SHEAR WALL WITH LOCATED OPENINGS

H.A. Jahangiry, M. Gholhaki[*, †] and M.K. Sharbatdar
Department of Civil Engineering, Semnan University, Semnan, Iran

ABSTRACT

This research focuses on the effects of stiffeners and architectural opening on the steel shear wall topology optimization. To this aim, four relevant issues have been considered. The first issue is the optimality Pattern of the shear wall without stiffeners. The second is the Optimality Pattern of the shear wall with stiffeners in two directions. The third is the investigation on the topology optimization of the shear walls with fixed opening and the fourth is the multi-material topology optimization of the above issues. In the optimize process, the level set method based on the shape sensitivity and the finite element analysis for two-dimensional linear elastic problems has been used. The level set function implicitly indicated the boundaries of the design domain. Several numerical examples are used to demonstrate the optimal paths in the steel shear walls. The results show that optimal values have been changed by replacing stiffeners and creating openings in the wall, but the optimal topologies almost have a shape like a concentric bracing. Also, in the conventional shear walls (one material) the horizontal stiffeners have a significant effect on their performance.

Keywords: multi-materials; topology optimization; steel shear wall; implicit function; level sets; reaction-diffusion equation; sensitivity analysis; tow directional stiffener; architectural opening.

Received: 12 September 2019; Accepted: 21 December 2019

1. INTRODUCTION

Generally, the goal of the structural topology optimization is to find the appropriate distribution of materials into a proposed design domain, so that the optimal structure has prominent characteristics. Topology optimization is a material distribution method which is used to optimize a structural design to minimize a specific objective function criterion under design constraints and a physical model. In the pioneering research by Prager and Rozvany [1], Cheng and Olhoff [2], Bendsøe and Kikuchi [3, 4], and Zhou and Rozvany [5],

[*]Corresponding author: Department of Civil Engineering, Semnan University, Semnan, Iran
[†]E-mail address: mgholhaki@semnan.ac.ir (M. Gholhaki)

Topology optimization has been attracted considerable attention. Multitude topology optimization methods have been introduced and applied in literatures. The homogenization Method using an infinite number of micro-scale holes which are periodically distributed in the fixed design domain, transforms the topology optimization problem into the size optimization problem [6]. In this way, the determinant parameters of these holes are considered as design variables in each element of FEM. Also, artificial materials are presented to eliminate grayscale areas in optimum layouts [7-10], which is called Solid Isotropic Material with Penalization (SIMP). Jahangiry and Tavakkoli [11], used a combination of IGA and LSM topology optimization for problems which include local stress constraints. Also, Jahangiry and Jahangiri [44], used a combination of IGA and LSM topology optimization for two-dimensional heat-transfer problems. In their work, the reaction-diffusion equation was used to update the design variables. It can be seen that most of the optimization methods and published articles are focused on the single-material optimization [12-16]. However, as explained in [17], most of the real-world engineering design issues include several materials. Wenjie and Kazuhiro [18] solved multi-material topology optimization problems with the SIMP method. Wang and Wang [19] used the level-set method in other to multi-material topology optimization. Gou et al. [20] have been investigated the stress constraints topology optimization in continuum structures, including multiple heterogeneous materials. Zhang et al. [21] representation a new approach in order to achieve optimized topology with multiple materials based on the Moving Morphable Component (MMC) framework, in which the MMC approach was proposed by Guo et al. [22] to solve topology optimization problems with a finite number of design variables. In the field-phase approach, the Cahn-Hilliard equation was used to solve the time-dependent equation [23, 24], which is a general method to solve the multiphase structural topology optimization problems. The multi-material level set (MMLS) based topology optimization was proposed by Mai and Wang [25] in which the mean curvature flows acts as a regularization term Also, the ‘color’ level set method was employed in compliant mechanisms [26], heterogeneous objects [27], heat conduction structures [28] and stress-constrained structures [29] problems. In [29, 30], the authors used precise shapes derivatives to optimize multi-phase topology. Recently, Vermaak et al. [31] introduced the continuous material property transition at the material interface and Liu et al. [32], investigated the correlation model. In addition, the multi-phase topology optimization has also been represented in the other frameworks, such as BESO (Bidirectional Evolutionary Structural Optimization) [33, 34] and phase fields [35, 36]. The multi-material topology optimization of the thermo-mechanical buckling constraints has been developed by C. Wu et al. [37]. In order to combine the thermal loads, a general thermal stress coefficient (TSC) was used to show the joint effects of Young's modulus, Poisson’s ratio and thermal expansion coefficient. In their work [38], a rational approximation of the material properties model (RAMP) was used to parameterize the multi-phase system of optimization. Jikai Liu and Yongsheng Ma [39] proposed a new level set based multi-material topology optimization. They introduced a new multi-material level set interpolation, in which overlapping regions are filled with an artificial weak material type and suppressed during the evolution process. Consequently, each material phase is represented by a single level set function. Therefore, the signed distance-based geometrical information is well preserved in each material phase which enables the independent length scale control. Hamid Ghasemi et al. [40] applied an

IGA multi-material level set-based topology optimization for the flexoelectric composites. Their work provides a new prospect on the simultaneous topology optimization of the elastic, flexoelectric and void phases in the design field, so that multi-material flexoelectric composites can be designed. Thanh Thien Banh and Dongkyu Lee [41], explained a multi-phase topology optimization scheme for the continuum structures with crack patterns. Their work provides a method to evaluate the mechanical and the numerical interaction between multi-material and cracked problem within topology optimization template, including distribution of the different materials in a prescribed cracked structure and how to generate the information of the reinforcement of the cracked structure.

Steel plate shear walls have been used in steel structures to withstand earthquake and wind forces. This system has many advantages compared to other conventional lateral load resisting systems. When used of stiffeners, they can effectively restrain the out-of-plane displacements and improve the shear strength and ductility. Since the preparation of such thin steel plates is simply not possible, a thicker plate is used with openings to reduce its stiffness [45]. On the other hand, the existence of opening is inevitable due to architectural considerations such as lighting. Also, it is sometimes necessary to introduce openings in the steel plate shear walls. This happens when the steel plate shear walls are used as windows in the facade panels. Kaveh and Farhadmanesh [46], investigated three well-known metaheuristic algorithms such as Colliding Bodies, Enhanced Colliding Bodies and Particle Swarm Optimization for size and performance optimization of the steel plate shear wall in multi-story systems. Kamgar et al. [47], investigated the effect of substituting the shape memory alloy (SMA) instead of steel on shear walls. Their results also show that composite of steel and shape memory alloy improve the performance of shear walls. Bagherinejad and Haghollahi [48, 49], used the topology optimization method to find the proper location of the openings. In their investigation, SIMP and MMA were used to parameterize the design variables and optimization, respectively. Therefore, this paper focuses on the multi-material optimality pattern of stiffened steel shear walls and investigation on optimality patterns of a stiffened steel shear wall with and without located openings in the design domain. For this purpose, in the topology optimization stage, the level set method with reaction-diffusion equation and in structural analysis phase, the finite element analysis has been used.

2. DESIGN REPRESENTATION AND OPTIMIZATION VIA LEVEL SET METHOD

In this section, the level set approach is briefly explained. If the Level Set method (LSM) [21] is used for topology optimization, it can be used of its intrinsic flexibility in dealing with topological changes. In LSM, domain boundaries are implicitly represented with a scalar hyper-surface in a higher dimension as a zero level set function which is changed over the time and provides unique advantages such as smooth boundaries and distinct interfaces, integrated shape and topology optimization. Therefore, any change in the $\phi(x)$ during the optimization process can lead to moving the boundaries, merging or splitting the holes inserted in the structure. For the first time, osher and Sethian (1988) proposed the level set method, which is an implicit interface modeling and tracking technique which has been successful in various engineering fields, including image processing, scanning,

computational fluid dynamics, and structural optimization, etc. An implicit level set function $\phi(x)$ can be defined as follows:

$$\begin{aligned} 0 < \phi(\mathbf{x}) \leq +1 \quad & \forall \mathbf{x} \in D \\ \phi(\mathbf{x}) = 0 \quad & \forall \mathbf{x} \in D \cap D \\ -1 \leq \phi(\mathbf{x}) < 0 \quad & \forall \mathbf{x} \in \overline{D} \end{aligned} \tag{1}$$

where D and $\overline{D}$ are solid and void regions, respectively and x can be any point in the design structure. The nodal values of the LSF are used to generate a smooth Heaviside function, Which is obtained from multiplying the density of the material at each integration point of the elements by the value of the smooth Heaviside function. Thus, the elemental stiffness matrix is expressed as follows:

$$K_e = \sum_{i=1}^{N_g} B_i^T C_i B_i w_i H(\phi(x_i)) \tag{2}$$

Where K_e, N_g, B_i, C_i and w_i are the element stiffness matrix, the number of integration points, strain displacement matrix, material stiffness matrix and integral weight at point i, respectively. In this work, in order to avoid numerical instability and singularity in stiffness matrices, the smooth Heaviside function and its derivative, Delta Dirac's function can be written as follows:

$$\begin{aligned} H(x) &= \begin{cases} \alpha & , \quad x \leq \Delta \\ \frac{1}{2}(1 + \sin(\frac{\pi x}{2\Delta})) & , \quad -\Delta < x < \Delta \\ 1 & , \quad x \geq \Delta \end{cases} \\ \delta(x) &= \frac{\partial H(x)}{\partial x} = \begin{cases} \frac{\pi}{4\Delta}\cos(\frac{\pi x}{2\Delta}) & , \ |x| \leq \Delta \\ 0 & , \ |x| > \Delta \end{cases} \end{aligned} \tag{3}$$

So that, α and Δ are small scalar values.

3. SENSITIVITY ANALYSIS

The strain energy *J,* minimization problem with a given amount of materials V_{max}, can be written as follows:

$$\begin{aligned} &\underset{\phi(x)}{Minimize} && J(\boldsymbol{u},\phi(\boldsymbol{x})) = \int_{\Omega} \tfrac{1}{2}\, \boldsymbol{u}^{\mathrm{T}} \boldsymbol{k}^{\mathrm{e}} \boldsymbol{u}\; H(\phi(\boldsymbol{x}))\, d\Omega \\ &Subject\ to: && equilibrium \\ & && volume constraint: V \le V_{\max} \\ & && design\ restrictions \end{aligned} \tag{4}$$

where $\boldsymbol{u}$ is the unknown displacement field and $\boldsymbol{k}^e$ is the elemental stiffness matrix and Ω represents the design domain. Accordingly, the unconstrained function of the above problem is expressed as follows:

$$L(\boldsymbol{u},\phi) = \frac{1}{2}\int_D \boldsymbol{u}^T \boldsymbol{k}^e \boldsymbol{u}\, H(\phi) d\Omega + \lambda \left(\int_D H(\phi) d\Omega - V_{\max}\right) \tag{5}$$

The sensitivity analysis of the objective function J and its constraints with respect to the node's positions are expressed as follows:

$$\frac{\partial J}{\partial \phi} = \boldsymbol{u}^T \boldsymbol{k}^e \frac{\partial \boldsymbol{u}}{\partial \phi} + \frac{1}{2}\boldsymbol{u}^T \frac{\partial \boldsymbol{k}^e}{\partial \phi}\boldsymbol{u} \tag{6}$$

Based on the direct method in sensitivity analysis, $\frac{\partial \mathbf{u}}{\partial \phi}$ might be calculated by differentiating both sides of an equilibrium equation of the element, i.e. $\boldsymbol{k}^e\boldsymbol{u}=\boldsymbol{f}$ with respect to the design variables and note that $\boldsymbol{f}$ is independent of the design variables, so it can be expressed that,

By differentiating from the equilibrium equation, i.e. $\boldsymbol{k}^e\boldsymbol{u}=\boldsymbol{f}$ with respect to the design variables, it can be expressed that:

$$\frac{\partial \boldsymbol{u}}{\partial \phi} = -\boldsymbol{k}^{e-1} \frac{\partial \boldsymbol{k}^e}{\partial \phi}\boldsymbol{u} \tag{7}$$

Substituting Eq. (7) into Eq. (6) gives:

$$\frac{\partial J}{\partial \phi} = -\frac{1}{2}\mathbf{u}^T \frac{\partial \mathbf{k}^e}{\partial \phi}\mathbf{u} \tag{8}$$

Also, the stiffness matrix of the element can be expressed as follows:

$$\mathbf{k}^e = \int_{\Omega^e} \mathbf{B}^T \mathbf{C}\mathbf{B}\, H(\phi) d\Omega^e \tag{9}$$

where, $H(\phi)$ provides the integration over the material domain. Differentiating by node's positions yields,

$$\frac{\partial \mathbf{k}^e}{\partial \phi} = \int_{\Omega^e} \mathbf{B}^T \mathbf{C} \mathbf{B}\, \delta(\phi) |\nabla \phi| d\Omega^e = \int_{\partial\Omega} \mathbf{B}^T \mathbf{C} \mathbf{B}\, ds \tag{10}$$

Therefore, combining Eq. (8) and Eq. (10) gives the derivation of the compliance function. Also, the derivative of the volume constraint V is expressed as follows:

$$\begin{aligned} V &= \int_{\Omega^e} H(\phi) d\Omega \\ \frac{\partial V}{\partial \phi} &= \int_{\Omega^e} \frac{\partial H(\phi)}{\partial \phi} d\Omega = \int_{\Omega^e} \delta(\phi) |\nabla \phi| d\Omega = \int_{\partial\Omega} 1\, ds \end{aligned} \tag{11}$$

where, $\partial\Omega$ denotes the structural boundaries. Therefore, the normal velocity field is expressed as follows:

$$v_n(\mathbf{x}) = -(-\frac{1}{2} \int_D \mathbf{u}^T \frac{\partial \mathbf{k}^e}{\partial \phi} \mathbf{u}\, H(\phi(\mathbf{x})) d\Omega + \lambda) \tag{12}$$

Also, the Lagrange multiplier of the volume constraint is expressed as:

$$\lambda = \frac{\int_D (\frac{1}{2} \boldsymbol{u}^T \boldsymbol{k}^e \boldsymbol{u}\, \delta(\phi) |\nabla \phi|)\, d\Omega}{\int_D \delta(\phi) |\nabla \phi|\, d\Omega} \tag{13}$$

Based on the KKT conditions, if λ gets negative from the above calculations, it must be equal to zero.

3.1 Multi-material level set interpolation

As regards that a single level set function can only detect two phases through positive and negative signs, in this way, multiple level set functions are combined to interpolate several materials phases. In this work, the new method explained in [39] has been used. According to this method, each level set function is related to a material phase and the overlapping of the level set functions is allowed, but the overlapping areas are penalized with artificial materials which are weaker than any material phase.

The multi-material interpolation is expressed in Eq. (14).

$$\begin{aligned} E(\phi(x)) = {} & H(\phi_1(x)) \left[1 - H(\phi_2(x))\right] E^1 + \\ & H(\phi_2(x)) \left[1 - H(\phi_1(x))\right] E^2 + \\ & 0.1 H(\phi_1(x)) H(\phi_2(x)) \left(E^1 + E^2\right) \end{aligned} \tag{14}$$

The derivation or sensitivity analysis of this multi-material interpolation is illustrated in Eq. (15).

$$\begin{aligned}\frac{\partial E}{\partial \phi_1} &= \left(\begin{matrix}\left[1 - H(\phi_2(x))\right]E^1 - H(\phi_2(x))E^2 + \\ 0.1H(\phi_2(x))\left(E^1 + E^2\right)\end{matrix}\right)\delta(\phi_1(x)) \\ \frac{\partial E}{\partial \phi_2} &= \left(\begin{matrix}\left[1 - H(\phi_1(x))\right]E^2 - H(\phi_1(x))E^1 + \\ 0.1H(\phi_1(x))\left(E^1 + E^2\right)\end{matrix}\right)\delta(\phi_2(x))\end{aligned} \tag{15}$$

3.2 Reaction-diffusion equation

As mentioned previously, the reaction-diffusion equation, presented in [42, 43 & 44], is used instead of the conventional Hamilton-Jacobi equation in the present work. The time evolution equation with initial and boundary conditions of this method can be summarized as follows:

$$\begin{cases}\dfrac{\partial \phi}{\partial t} = v_n(\phi) + \tau\Delta\phi & , \quad in \quad \Omega \\ \phi(t=0) = \phi_0 & , \quad in \quad \Omega \bigcup \partial\Omega \\ \nabla\phi.n = \dfrac{\partial \phi}{\partial n} & , \; on \quad \partial\Omega \setminus \partial\Omega_N \\ \phi = 1 & , \quad on \quad \partial\Omega_N \\ n = \dfrac{\nabla\phi}{|\nabla\phi|}\end{cases} \tag{16}$$

where, Δ denotes the Laplacian operator and τ is a positive diffusion coefficient term that controls the effect of regularization. Also, τ is used to assure that solutions exist and geometric constraints are applied. For this purpose, it could be used of fourth-order accurate finite difference approximation. The first line of Eq. (16) is the reaction-diffusion equation which is known as an Allen–Cahn equation [42, 43, 44, & 45], Which is used in the phase-field method.

4. NUMERICAL INVESTIGATIONS

In this section, numerical examples will be investigated. Generally, three types of problem are explained. The first is the square domain which its aspect ratio (H/L) is equal to 1, the second is the rectangular domain which its aspect ratio is equal to 2 and the Third is the rectangular domain which its aspect ratio is equal to 0.5.

In all examples, the modulus of elasticity and the Poisson's ratio of the strong (■) materials are considered as 1 *Pa* and 0.34, respectively. Also, in the multi-material topology optimization problems, the modulus of elasticity and the Poisson's ratio of the weak (■) materials are considered as 0.1 Pa and 0.20, respectively.

The concentrated load value is assumed to be P=1 *N*. The narrow bandwidth transition for the Heaviside function is considered as $\Delta = 1.0$. Also, the time step is considered $\Delta t = \frac{0.3 \min\{\Delta x, \Delta y\}}{|v_{\max}|}$. Where, v_{max} is the maximum velocity over the boundaries and Δx and Δy are the nodal distances in x and y-direction, respectively. Also, α in Eq. (3) is set to 1e−4. The regularization parameter τ is set to 1e−6. Also, the material volume fraction is equal to 40% for strong material and 20% for weak material of the entire volume of the structure for all problems. In all examples, the stiffness of the external frame is 100 times and the stiffness of the stiffeners is 10 times the shear wall stiffness.

Example 1. A cantilever shear wall subjected to the concentrated loads at the end corners is considered as shown in Fig. 1. The H/L ratio equals 1, where L=1 m and H=1 m. In order to discretize the design domain, 1600 four-node elements, including 1681 nodes are employed and the nodal distances in x and y direction are Δx = Δy = 0.025m, respectively. Also, specific characteristics of architectural opening are demonstrated in Fig. 1.

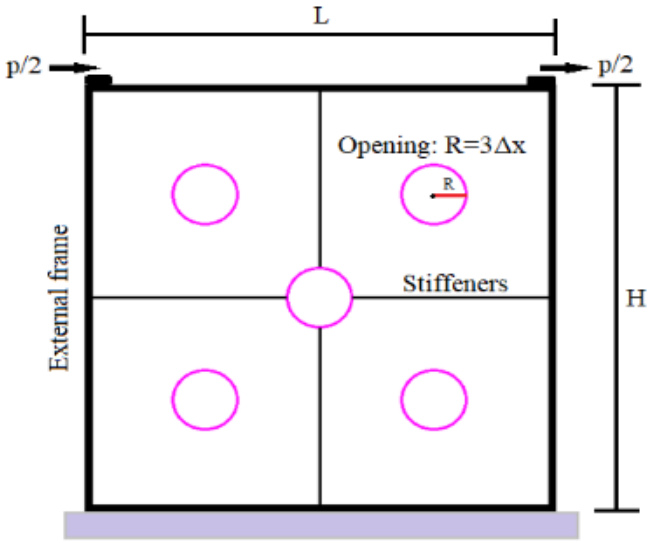

Figure 1. The design domain, loading and boundary condition of Example 1

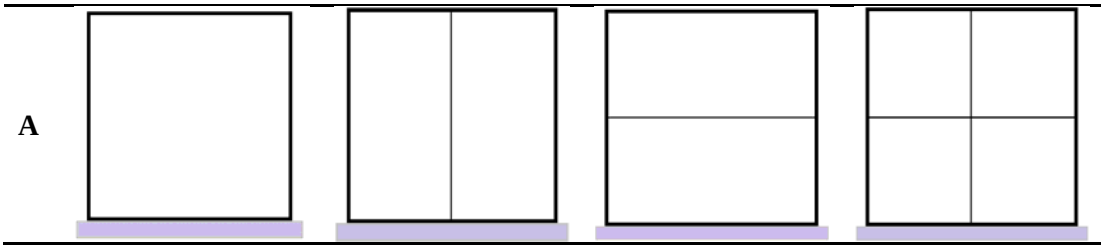

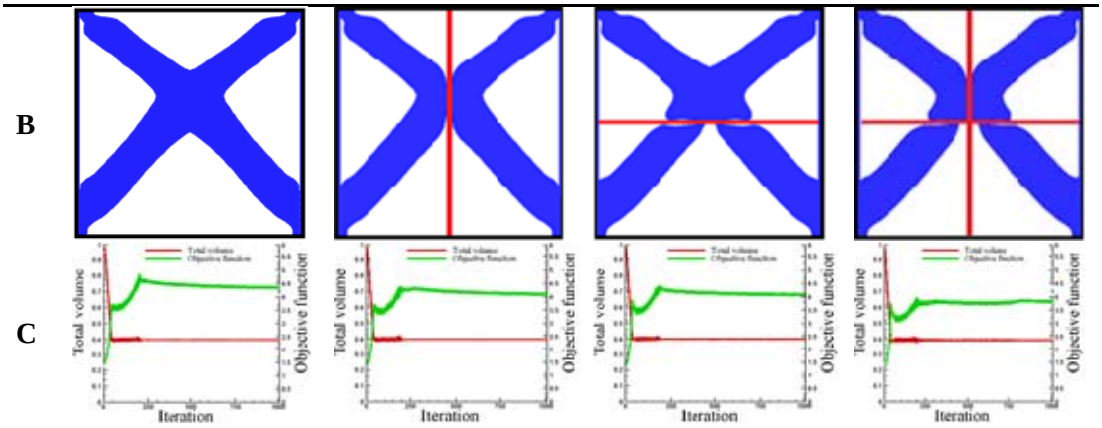

Objective Function: 4.42 4.11 4.08 3.89

Figure 2. (A) The stiffener pattern, (B) optimum layouts and (C) convergence history of the objective function and volume constraint for Example 1

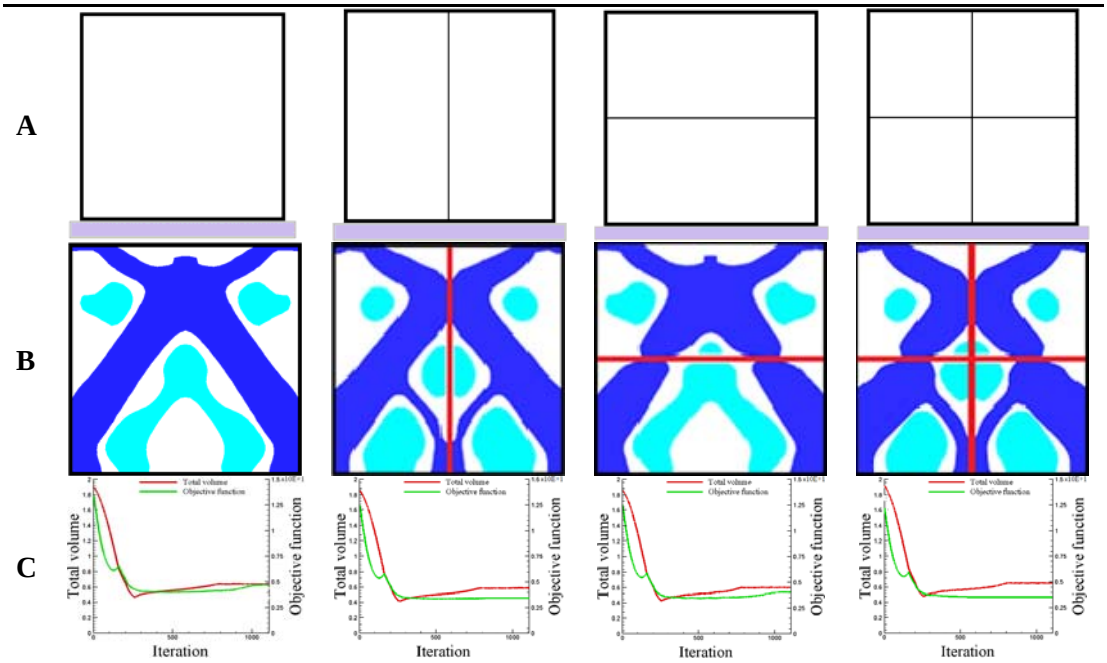

Objective Function: 4.42 3.87 3.96 3.56

Figure 3. (A) The stiffener pattern, (B) optimum layouts and (C) convergence history of the objective function and volume constraint for Example 1

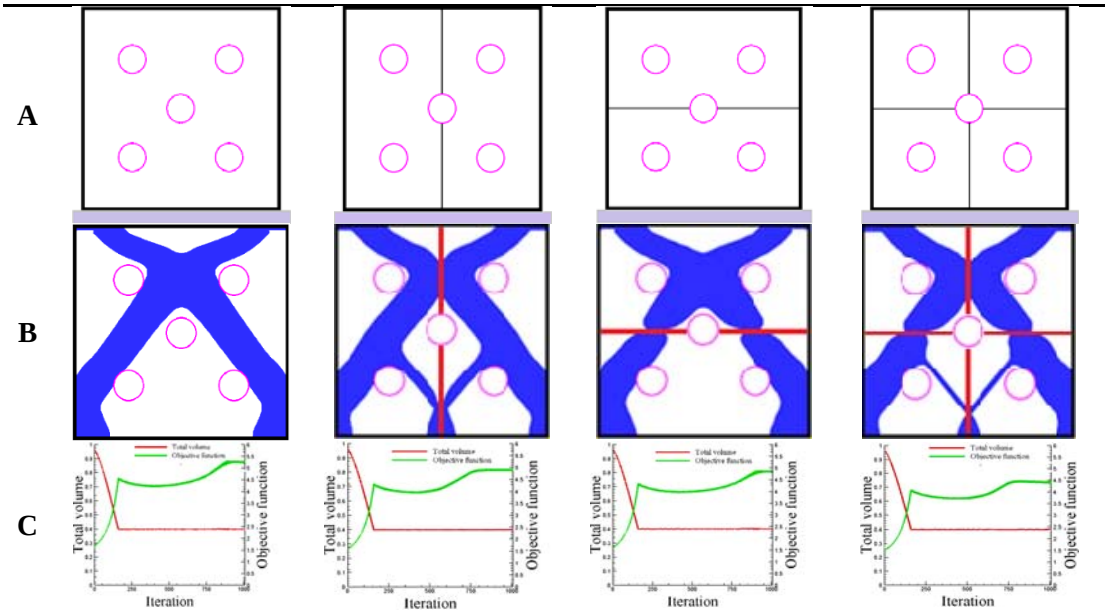

Figure 4. (A) The stiffener pattern and located openings, (B) optimum layouts and (C) convergence history of the objective function and volume constraint for Example 1

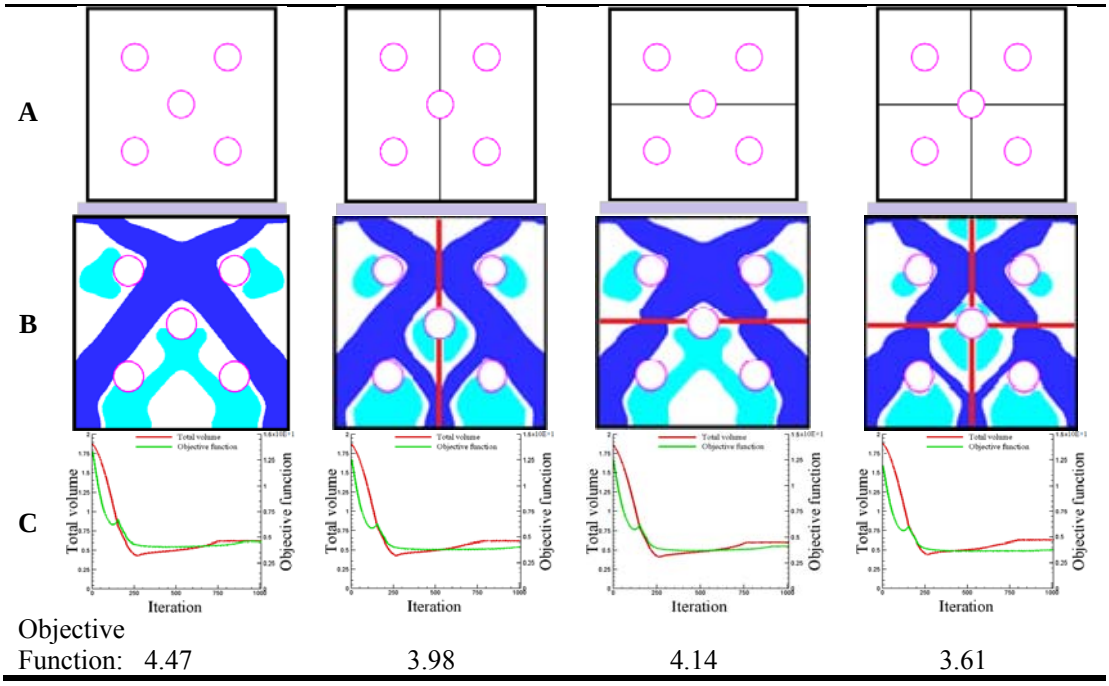

Figure 5. (A) The stiffener pattern and located openings, (B) optimum layouts and (C) convergence history of the objective function and volume constraint for Example 1

From the results, it has been observed that, the horizontal stiffeners do not affect the final topology, but the vertical stiffeners adjust the optimized layout, appropriately. It is also observed that in the square domain whose aspect ratio is equal to 1, in the one material topology optimization, the horizontal stiffeners have a significant effect on the performance of the optimized shear wall, but in the multi-material topology optimization, the vertical stiffeners have a significant effect on the performance of the optimized shear wall. Figs. 2-5 (B) and 2-5 (C), illustrate the final layout and the iteration history of this optimization problem, respectively.

Example 2. A cantilever shear wall subjected to the concentrated loads at the end corners is considered as shown in Fig. 6. The H/L ratio is equal to 2, where L=0.5 m and H=1 m. In order to discretize the design domain, 800 four-node elements, including 861 nodes are employed and the nodal distances in x and y direction are $\Delta x = \Delta y = 0.025$m, respectively. Also, specific characteristics of architectural opening are illustrated in Fig. 6.

From the results, it has been observed that in the rectangular domain whose aspect ratio is equal to 2, in all topology optimization problems, the existence of stiffeners and openings do not much effect on the final topology. It is also observed that, in the one material topology optimization, the horizontal stiffeners have a significant effect on the performance of the optimized shear wall, but in the multi-material topology optimization, the vertical stiffeners have a significant effect on the performance of the optimized shear wall. Figs. 7-10 (B) and (7-10) (C), illustrate the final layout and the iteration history of this optimization problem, respectively.

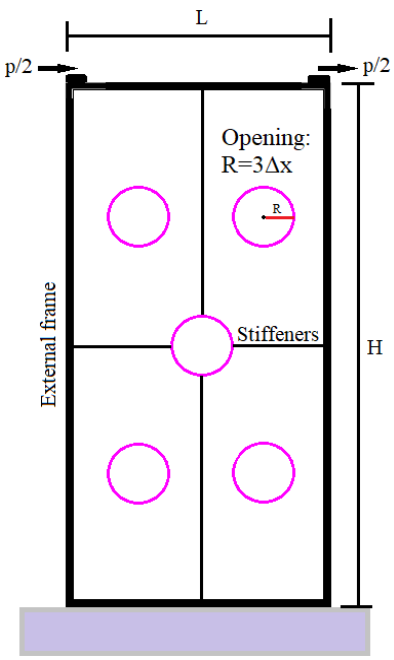

Figure 6. The design domain, loading and boundary condition of Example 2

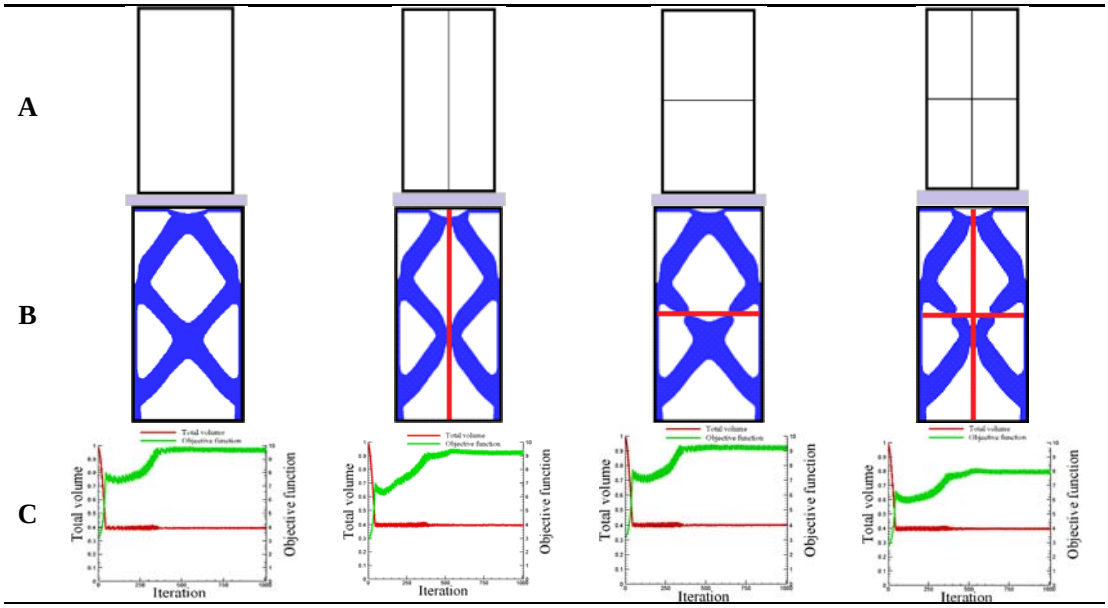

Objective Function:	9.82	9.13	8.94	7.84

Figure 7. (A) The stiffener pattern, (B) optimum layouts and (C) convergence history of the objective function and volume constraint for Example 2

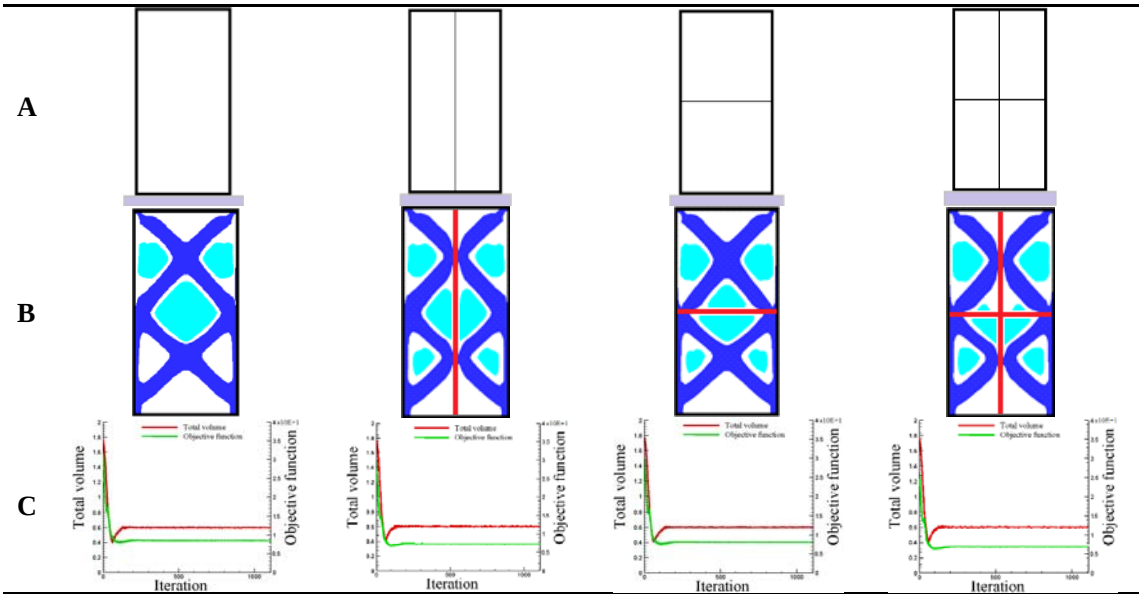

Objective Function:	8.47	7.76	8.06	7.42

Figure 8. (A) The stiffener pattern, (B) optimum layouts and (C) convergence history of the objective function and volume constraint for Example 2

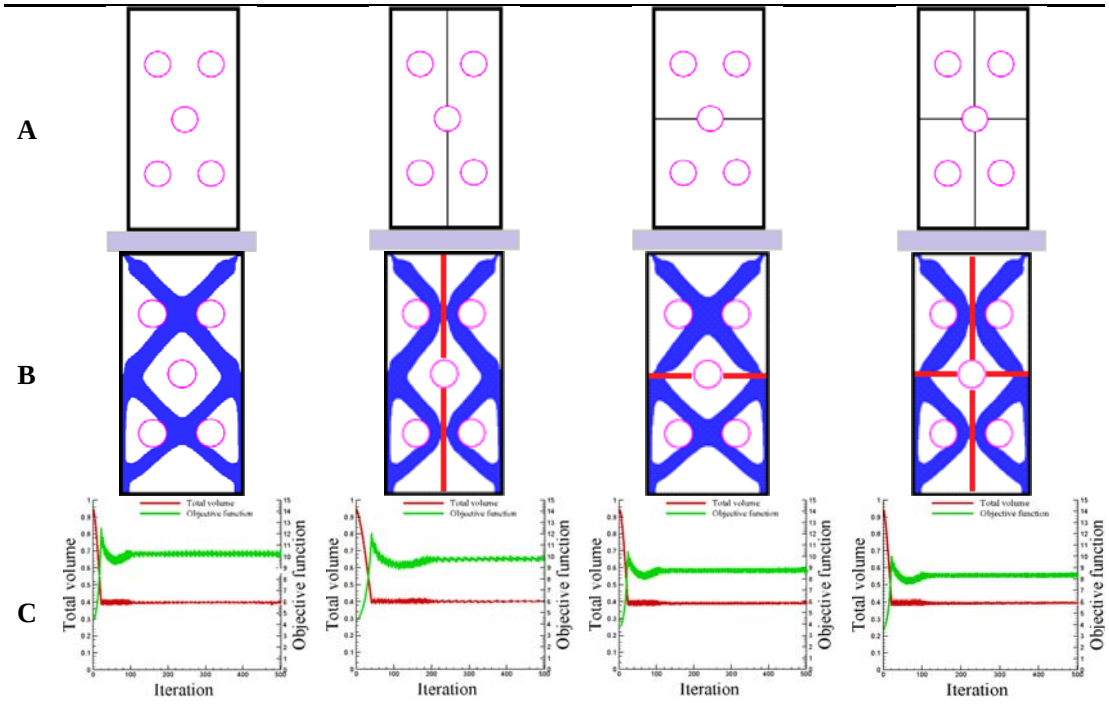

Objective Function:	10.12	9.69	8.96	8.47

Figure 9. (A) The stiffener pattern and located openings, (B) optimum layouts and (C) convergence history of the objective function and volume constraint for Example 2

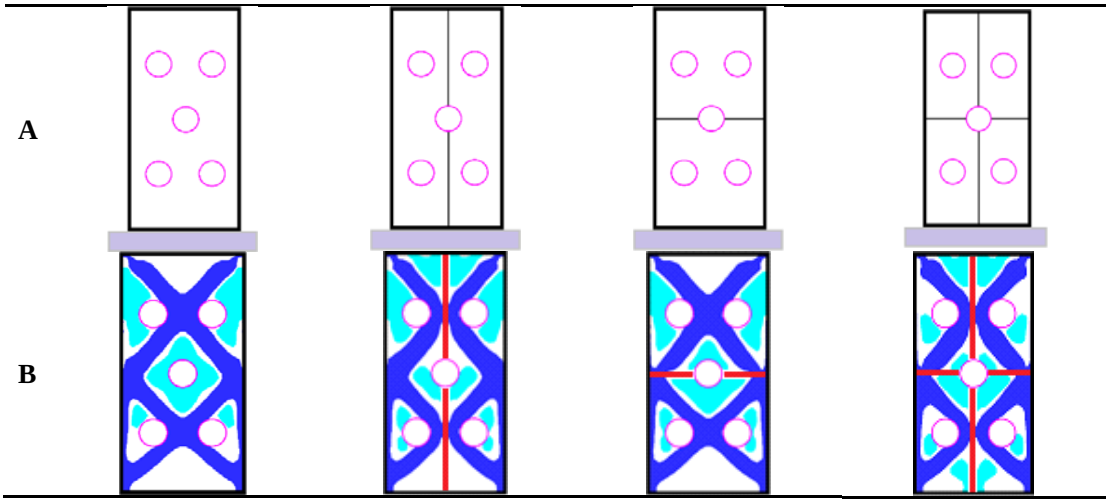

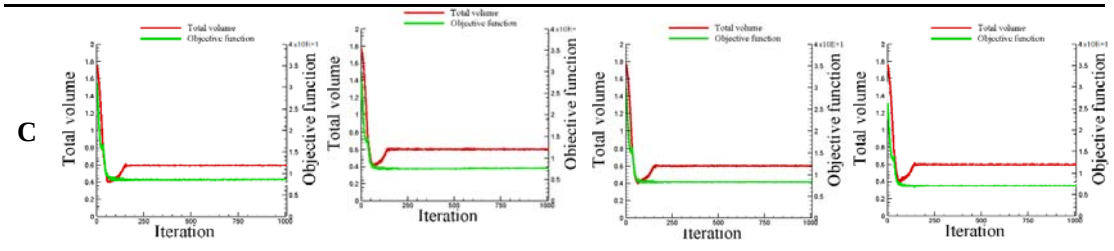

Figure 10. (A) The stiffener pattern and located openings, (B) optimum layouts and (C) convergence history of the objective function and volume constraint for Example 2

Example 3. A cantilever shear wall subjected to the concentrated loads at the end corners is considered as shown in Fig. 11. The H/L ratio is equal to 0.5, where L=1 m and H=0.5 m. In order to discretize the design domain, 800 four-node elements, including 861 nodes are employed and the nodal distances in x and y direction are $\Delta x = \Delta y = 0.025$m, respectively. Also, specific characteristics of architectural opening are illustrated in Fig. 11.

From the results, it can be observed that in the rectangular domain which its aspect ratio is equal to 0.5, the horizontal stiffeners do not affect the final topology, but the vertical stiffeners change the optimized layout, appropriately. It is also observed that in the square domain whose aspect ratio is equal to 1, in the one material topology optimization, the horizontal stiffeners have a significant effect on the performance of the optimized shear wall, but in the multi-material topology optimization, the vertical stiffeners have a significant effect on the performance of the optimized shear wall. Figs. 12-15 (B) and 12-15 (C), illustrate the final layout and the iteration history of this optimization problem, respectively.

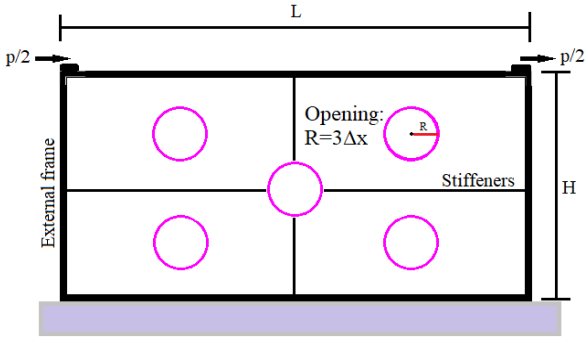

Figure 11. The design domain, loading and boundary condition of Example 3

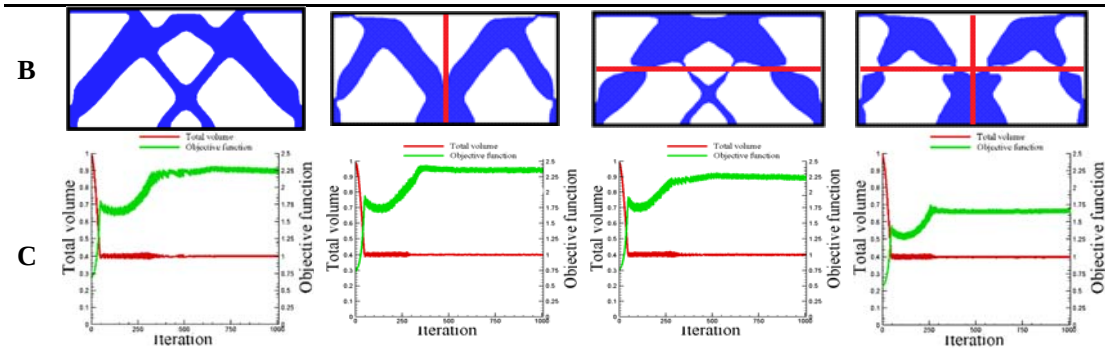

Objective Function:	2.28	2.13	1.93	1.67

Figure 12. (A) The stiffener pattern, (B) optimum layouts and (C) Iteration history of objective function and volume for Example 3

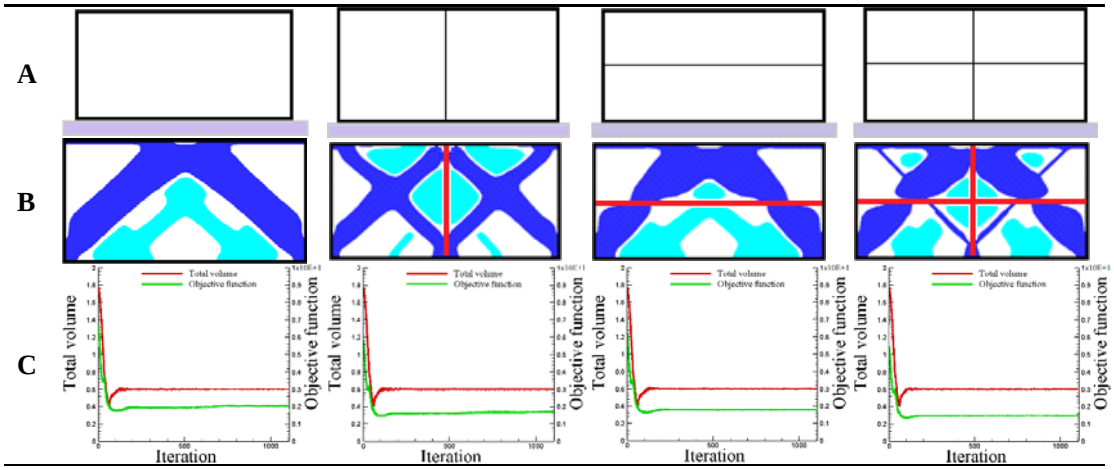

Objective Function:	2.03	1.78	1.82	1.56

Figure 13. (A) The stiffener pattern, (B) optimum layouts and (C) Iteration history of objective function and volume for Example 3

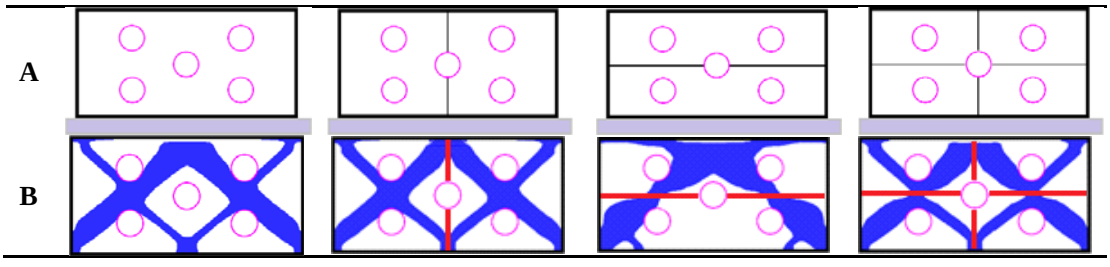

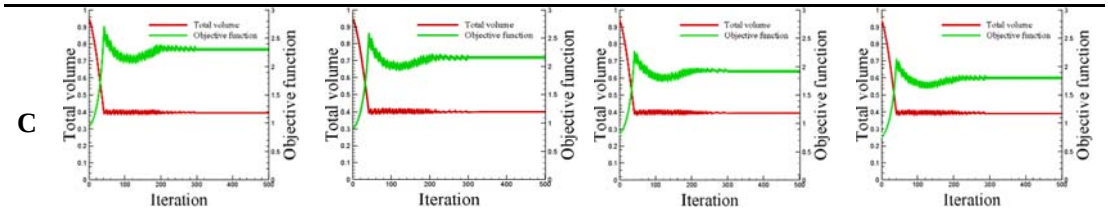

Objective Function:	2.31	2.28	2.12	1.89

Figure 14. (A) The stiffener pattern and located openings, (B) optimum layouts and (C) Iteration history of objective function and volume for Example 3

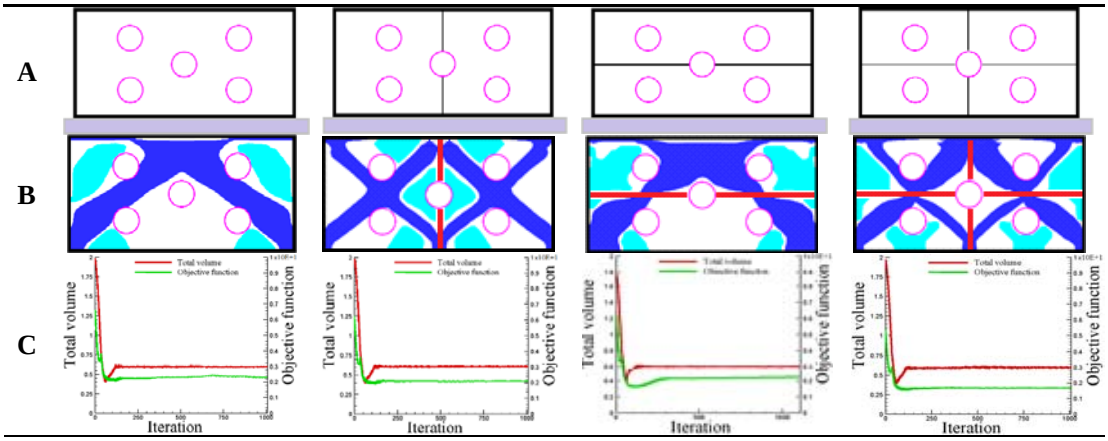

Objective Function:	2.25	2.05	2.09	1.77

Figure 15. (A) The stiffener pattern and located openings, (B) optimum layouts and (C) Iteration history of objective function and volume for Example 3

5. CONCLUSIONS

In this paper, the level set method is considered to form the topology of structure so that the zero contour of the function indicates the boundaries of the structure. Several steel shear walls are implemented as numerical examples to investigate the optimal pattern in which have various aspect ratios. For this purpose, at first, an optimal topology for each aspect ratio was obtained without any stiffeners. A second, by replacing the stiffeners in different directions, the changes in optimal topology and the magnitude of the objective function were investigated. A third, the optimal topology and value of the objective function in the multi-material shear wall with and without stiffeners were also investigated for all examples mentioned above. A fourth, by replacing the architectural openings in the shear walls, the changes in the optimal topology and the value of the objective function were investigated in all samples. It should be noted that minimizing the strain energy, increases the structural stiffness and consequently, reduces the lateral displacements. Therefore, using the multi-

material shear walls, decreased the strain energy and then, reduce the lateral displacements. Also, replacement of the architectural openings within the shear walls, due to the deviation of the optimal patterns from the openings, increased the strain energy. It should be noted that the external frame and the stiffeners are specified in black and red colors in optimal layouts, respectively. Also, the design variables related to the external frame and the stiffeners are considered inactive. This means that they will have no variation during the optimization process. According to this experience, reducing the aspect ratio increased the effect of stiffeners on the final layout and with a lateral loading, in the one material topology optimization, the horizontal stiffeners have more performance than vertical stiffeners, but in the multi-material topology optimization, it has been observed that the vertical stiffeners have more performance. However, using both horizontal and vertical stiffeners simultaneously creates the best conditions. Also, almost all optimal topologies will have a pattern similar to the concentric bracing.

REFERENCES

1. Prager W, Rozvany GIN. Optimal layout of grillages, *J Struct Mech* 1977; **5**(1): 1–18. DOI: 10.1080/03601217708907301.
2. Cheng KT, Olhoff N. An investigation concerning optimal design of solid elastic plates, *Int J Solid Struct* 1981; **17**(3): 305–23. DOI: 10. 1016/0020-7683(81)90065-2.
3. Bendsøe MP, Kikuchi N. Generating optimal topologies in structural design using a homogenization method, *Comput Meth Appl Mech Eng* 1988; **71**(2): 197-224. DOI: 10.1016/0045-7825 (88) 90086-2.
4. Bendsøe MP. Optimal shape design as a material distribution problem, Structural optimization 1 (4) (1989) 193–202. DOI: 10.1007/bf01650949.
5. Zhou M, Rozvany GIN. The COC algorithm, part II: Topological, geometrical and generalized shape optimization, *Comput Meth Appl Mech Eng* 1991; **89**(1): 309-36. DOI: 10.1016/0045-7825 (91) 90046-9.
6. Hassani B, Hinton E. *Homogenization and Structural Topology Optimization: Theory, Practice and Software*, Springer, London, UK, 1999.
7. Bendsøe MP. Optimal shape design as a material distribution problem, *Struct Optim* 1989; 1: 193–202. DOI: 10.1007/BF01650949.
8. Rozvany GIN. *Structural Design via Optimality Criteria*, Kluwer Academic Publishers, Dordrecht, 1989.
9. Rozvany GIN, Zhou M. The COC algorithm, part I: Cross-section optimization or sizing, Comput, *Methods Appl Mech Eng* 1991; **89**: 281–308. DOI: 10.1016/0045-7825(91)90045-8.
10. Bendsøe MP, Sigmund O. *Topology Optimization: Theory, Methods, and Applications*, 2003. DOI:10.1063/1.3278595.
11. Jahangiry HA, Tavakkoli SM. An isogeometrical approach to structural level set topology optimization, *Comput Meth Appl Mech Eng* 2017; **319**: 240-57.
12. Bendsoe MP, Sigmund O. *Topology Optimization: Theory, Methods, and Applications*, Springer, 2003.

13. Rozvany GI. A critical review of established methods of structural topology optimization, *Struct Multidisc Optim* 2009; **37**(3): 217-37.
14. Sigmund O, Maute K. Topology optimization approaches, *Struct Multidisc Optim* 2013; **48**(6): 1031-55.
15. van Dijk NP, Maute K, Langelaar M, Van Keulen F. Level-set methods for structural topology optimization: a review, *Struct Multidisc Optim* 2013; **48**(3): 437–72.
16. Xia L, Xia Q, Huang X, Xie YM. Bi-directional evolutionary structural optimization on advanced structures and materials: a comprehensive review, *Archiv Computat Meth Eng* 2016, 1–42.
17. Chickermane H, Gea H. Design of multi-component structural systems for optimal layout topology and joint locations, *Eng Comput* 1997; **13**(4): 235-43.
18. Wenjie Z, Kazuhiro S. Multi-material topology optimization using ordered simp interpolation, *Struct Multidisc Optim* 2017; **55**: 477-491.
19. Wang MY, Wang X. "color" level sets: a multi-phase method for structural topology optimization with multiple materials, *Compu Meth Appl Mech Eng* 2004; **193**: 469-96.
20. Guo X, Zhang W, Zhong W. Stress-related topology optimization of continuum structures involving multi-phase materials, *Comput Meth Appl Mech Eng* 2014; 268:632-655.
21. Zhang W, Song J, Zhou J, Du Z, Zhu Y, Sun Z, Guo X. Topology optimization with multiple materials via moving morphable component (mmc) method, *Int J Numer Meth Eng* 2017; DOI: 10.1002/nme.5714.
22. Guo X, Zhang W, Zhong W. DOIng topology optimization explicitly and geometrically a new moving morphable components based framework, *J Appl Mech* 2014; **81**: 081009.
23. Zhou S, Wang M. Multimaterial structural topology optimization with a generalized cahn-hilliard model of multiphase transition, *Struct Multidisc Optim* 2006; **33**: 89-111.
24. Zhou S, Wang M. 3d multi-material structural topology optimization with the generalized cahn-hilliard equations, *Comput Model Eng Sci* 2006; **16**: 83-101.
25. Mei Y, Wang X. A level set method for structural topology optimization with multi-constraints and multi-materials, *Acta Mech Sin* 2004; **20**: 507–518. DOI: 10.1007/BF02484273.
26. Wang MY, Chen S, Wang X, Mei Y. Design of multi-material compliant mechanisms using level-set methods, *J Mech Des* 2005; **127**: 941–956. DOI:10.1115/1.1909206.
27. Wang MY, Wang X. A level-set based variational method for design and optimization of heterogeneous objects, *Comput Aided Des 2005*; 37: 321-37.
28. DOI:10.1016/j.cad.2004.03.007.
29. Zhuang C, Xiong Z, Ding H. Topology optimization of multi-material for the heat conduction problem based on the level set method, *Eng Optim* 2010; **42**: 811-31. DOI:10.1080/03052150903443780.25.
30. Guo X, Zhang W, Zhong W. Stress-related topology optimization of continuum structures involving multi-phase materials, *Comput Meth Appl Mech Eng* 2014; 268: 632-55. DOI:10.1016/j.cma.2013.10.003.
31. Allaire G, Dapogny C, Delgado G, Michailidis G. Multi-phase structural optimization via a level set method, *ESAIM Control Optim Calcul Variat* 2014; **20**: 576–611.
32. Vermaak N, Michailidis G, Parry G, Estevez R, Allaire G, Bréchet Y. Material interface effects on the topology optimization of multi-phase structures using a level set method, *Struct Multidisc Optim* 2014; **50**: 623-44. DOI: 10.1007/s00158-014-1074-2.

33. Liu P, Luo Y, Kang Z. Multi-material topology optimization considering interface behavior via XFEM and level set method, *Comput Meth Appl Mech Eng* 2016; 308: 113-33. DOI:10.1016/j.cma.2016.05.016.
34. Ghabraie K. An improved soft-kill BESO algorithm for optimal distribution of single or multiple material phases, *Struct Multidisc Optim* 2015; **52**: 773-90. DOI: 10.1007/s00158-015-1268-2.
35. Huang X, Xie YM. Bi-directional evolutionary topology optimization of continuum structures with one or multiple materials, *Comput Mech* 2009; **43**: 393. DOI: 10.1007/s00466-008-0312-0.
36. Zhou S, Wang MY. Multimaterial structural topology optimization with a generalized Cahn– Hilliard model of multiphase transition, *Struct Multidisc Optim* 2007; **33**: 89. DOI: 10.1007/s00158-006-0035-9.
37. Tavakoli R. Multimaterial topology optimization by volume constrained Allen–Cahn system and regularized projected steepest descent method, *Comput Meth Appl Mech Eng* 2014; 276: 534-65. DOI:10.1016/j.cma.2014.04.005.
38. Wu C, Fang J, Li Q. Multi-material topology optimization for thermal buckling criteria, *Comput Meth Appl Mech Eng* 2018; DOI: 10.1016/j.cma.2018.08.015
39. Stolpe M, Svanberg K. An alternative interpolation scheme for minimum compliance topology optimization, *Struct Multidisc Optim* 2001; **22**: 116-24.
40. Jikai L, Yongsheng M. A new multi-material level set topology optimization method with the length scale control capability, *Comput Meth Appl Mech Eng* 2018; **329**: 444-63.
41. Ghasemi H, Park HS, Rabczuk T. A multi-material level set-based topology optimization of flexoelectric composites, *Comput Meth Appl Mech Eng* 2017; DOI: 10.1016/j.cma.2017.12.005.
42. Banh TT, Lee D. Multi-material topology optimization design for continuum structures with crack patterns, *Compos Struct* 2017; DOI: 10.1016/j.compstruct.2017.11.088.
43. Yamada T, Izui K, Nishiwaki S, Takezawa A. A topology optimization method based on the level set method incorporating a fictitious interface energy, *Comput Meth Appl Mech Eng* 2010; **199**: 2876-91.
44. Emmendoerfer H, Fancello EA. Topology optimization with local stress constraint based on level set evolution via Reaction-Diffusion, *Comput Meth Appl Mech Eng* 2016; **305**: 62-88.
45. Jahangiry HA, Jahangiri A. Combination of Isogeometric analysis and level-set method in topology optimization of heat-conduction systems, *Appl Thermal Eng* 2019; **161**: 114134.
46. Afshari MJ, Gholhaki M. Shear strength degradation of steel plate shear walls with optional located opening, *Archives Civil Mech Eng* 2018; **18**(4): 1547-61.
47. Kaveh A, Farhadmanesh M. Optimal seismic design of steel plate shear walls using metaheuristic algorithms, *Period Polytech Civil Eng* 2019; **63**(1): 1-7.
48. Kamgar R, Askari Dolatabad Y, Babadaei Samani M. Seismic optimization of steel shear wall using shape memory alloy, *Int J Optim Civ Eng* 2019; **9**(4): 671-87.
49. Bagherinejad MH, Haghollahi A. Topology optimization of steel plate shear walls in the moment frames, *Steel Compos Struct* 2018; **29**(6): 771-83.
50. Bagherinejad MH, Haghollahi A. Topology optimization of perforated steel plate shear walls with thick plate in simple frames, *Int J Optim Civil Eng* 2019; **9**(3): 457-82.